Smallest Organic Tetracation in the Gas Phase: Stability of Multiply Charged Diiodoacetylene Produced in Intense Femtosecond Laser Fields

Takashi Kawaguchi, Kosei Kitagawa, Kazuo Toyota, Masatoshi Kozaki, Keiji Okada, Nobuaki Nakashima, Tomoyuki Yatsuhashi

Smallest Organic Tetracation in Gas Phase: Stability of Multiply Charged Diiodoacetylene Produced in Intense Femtosecond Laser Fields

Takashi Kawaguchi, Kosei Kitagawa, Kazuo Toyota, Masatoshi Kozaki, Keiji Okada,*[†]

*Nobuaki Nakashima, Tomoyuki Yatsuhashi**

Department of Chemistry, Graduate School of Science, Osaka City University, 3-3-138 Sugimoto, Sumiyoshi-ku, Osaka 558-8585 Japan

[*] To whom correspondence should be addressed. Telephone: +81-6-6605-2554. FAX: +81-6-6605-2552. E-mail: tomo@osaka-cu.ac.jp (T.Y.)

[†]Deceased 19 April 2019

ABSTRACT

Coulomb explosion imaging, which is the reconstruction of a molecular structure by measuring the three-dimensional momenta of atomic ions formed by a Coulomb explosion of multiply charged molecular cations (MMCs), has been utilized widely. In contrast, intact MMCs, whose properties and reactions are interesting from both fundamental and applied scientific perspectives, themselves have been little explored to date. This study demonstrates that the four-atom molecule diiodoacetylene (DIA) can survive as a long-lived species in the gas phase after the removal of four electrons in intense femtosecond laser fields. The electron configurations of the equilibrium structures of the electronic ground states calculated by the complete active space self-consistent-field (CASSCF) method reveal the stability of a multiply charged DIA. The dissociation energies are estimated to be 3.01, 3.59, 2.57, 1.82, and 1.61 eV for neutral, cation radical, dication, trication radical, and tetracation, respectively. A fairly deep potential well suggests that DIA tetracation is metastable toward dissociation, whereas the repulsive potential of pentacation radical confirms its absence in the mass spectrum. With their sufficiently long lifetimes, minimal numbers of atoms, and simple dissociation paths, DIA

MMCs are promising candidates for further experimental and theoretical investigations of multiply charged ion chemistry.

1. INTRODUCTION

Intense femtosecond laser pulses and/or collision with a highly charged atomic ion can strip many electrons from molecules followed by the production of atomic ions by Coulomb explosion.[1-2] The measurements of the three-dimensional momenta of those ions enable us to determine the static molecular structures[3] and to trace the molecular dynamics[4-7] of ultrafast chemical reactions. Although Coulomb explosion imaging has been widely utilized, intact multiply charged molecular cations (MMCs),[8] whose properties and reactions are interesting from both fundamental and applied scientific perspectives,[9-12] themselves have been little explored to date. As for theoretical studies, dications[13] have been studied, but there have been few theoretical reports about MMCs with charge numbers higher than three.[14-21] Dications and a few trication radicals whose lifetimes are sufficient for mass spectroscopic detection in the gas phase have been reviewed.[22-23] If the charge number increases and/or the molecular size decreases, MMCs are expected to be unstable because the Coulomb repulsions within the

molecular framework become stronger. Tetracations have rarely been reported by electron ionization,[24-26] but we have shown that several tetracations[27-31] and a pentacation radical[32] of organic molecules can be produced by sequential tunnel ionization in the strong alternating electric fields of an intense femtosecond laser. Among the tetracations ever reported, the diiodoacetylene (DIA) tetracation should be highlighted because it is hardly possible to imagine in the usual sense that such a four-atom molecule can survive after the removal of four electrons. In 2016, using density functional theory (DFT) calculations, we demonstrated that the localization (>90%) of the positive charges on the terminal iodine atoms, ensuring minimum Coulomb repulsion between adjacent atoms, enables the tetracation of DIA to remain metastable towards dissociation.[29] DFT calculations gave qualitative and, in part, quantitative explanations of the stability of the equilibrium structures of DIA MMCs. However, to further understanding the stability of DIA MMCs, more information is needed about the potential energy curves along a bond dissociation coordinate and hence about the dissociation energies as well as the details of electron configurations.

In this study, we estimated the lower limit of the lifetime of a multiply charged DIA by time-of-flight mass spectroscopy and ion trajectory simulations. In addition, the

electron configurations of the equilibrium structures of the electronic ground states calculated by the complete active space self-consistent-field (CASSCF) method[33] revealed the stability of a multiply charged DIA. Potential energy curves calculated along a C-I bond revealed the charge separation reactions of DIA MMCs. The dissociation energy along a C-I bond was calculated to be 1.6 eV for tetracation, whereas pentacation was unstable due to its repulsive nature. Positive charges were localized on the terminal iodine atoms at equilibrium configuration to minimize the Coulomb repulsions, and the charge redistribution was observed when the C-I bond was elongated.

2. METHODS

2.1 Ionization. DIA was prepared according to the reported method.[34] Xenon was purchased from Japan Air Gases with a stated purity of 99.99%. The experimental details have been described elsewhere.[35] Briefly, multiple ionization of DIA and xenon was carried out using a linearly polarized 40-fs pulse centered at 0.8 μm delivered from a 1-kHz-repetition-rate Ti:Sapphire laser (Alpha 100/1000/XS hybrid, Thales Laser), and the ions were detected by a Wiley−McLaren time-of-flight mass spectrometer equipped with a curved-field reflectron (refTOF-MS, KNTOF-1800, TOYAMA) as

described elsewhere.[36] The laser beam was focused into the ionization chamber with a plano-convex quartz lens with a 200-mm focal length. The position of the lens along the laser propagation direction was adjusted so as to maximize the signal intensity of the highest charge state of xenon observed (Xe^{5+}). We determined the actual laser intensity of the linearly polarized pulse at the focus by measuring the saturation intensity of xenon (1.1×10^{14} W cm^{-2} for a 45-fs pulse) by the method of Hankin et al.,[37] and the error in the determination of the absolute laser intensity was approx. ±10%. The DIA ions were measured successively after the measurement of saturation intensity of xenon without changing the experimental conditions between runs. The laser polarization direction was parallel to the ion flight axis. The output signal from the microchannel plate (MCP, F4655-11X; Hamamatsu Photonics) was averaged by a digital oscilloscope (Wave Runner 6100, 1 GHz; LeCroy Japan) for 1000 shots.

2.2. Computational Details. To avoid spin contamination and to consider near-degeneracy electron correlations, we carried out CASSCF calculations.[33] The initial geometries of DIA were prepared at the hybrid density-functional B3LYP level with the 6-31G basis set. The geometries were then reoptimized by the CASSCF method with the 6-311G* basis set. The GAMESS program was used to carry out all computations in

the present study.[38] The full-valence CASSCF includes a full-configuration interaction treatment of the 16 electrons in the active space of 12 orbitals in the cases of neutral DIA: 8 π orbitals and 4 σ orbitals, whereas lower orbitals were kept doubly occupied and frozen. For the cases of cation radical, dication, trication radical, tetracation, and pentacation radical, there were 15, 14, 13, 12, and 11 electrons in active spaces. For simplicity, we denote the molecular orbitals used for the active space of DIA as, from lower to higher energy, bonding σ orbitals in C-I bonds (1σ, 2σ), superimposed π orbitals in C-I and C-C bonds (1π, 2π), lone-pair orbitals on I atoms (3π, 4π), superimposed orbitals of bonding π orbitals in a C-C bond and lone-pair orbitals on I atoms (5π, 6π), antibonding σ orbitals in C-I bonds (3σ, 4σ), and antibonding π orbitals in a C-C bond (7π, 8π). The numbers of configurations (determinants) used in the present CASSCF calculation of neutral, cation radical, dication, trication radical, and tetracation were 61473, 97976, 114464, 183008, 214032, and 183008, respectively.

3. RESULTS AND DISCUSSION

3.1. Estimation of the Lifetime (Lower Limit) of MMCs. Figure 1 shows the time-of-flight and mass spectra of DIA observed by using refTOF-MS. As previously demonstrated using a linear TOF-MS (a reflectron was not used),[29] atomic ions and

molecular ions (DIA^{z+}, z = 1−4) were dominantly observed. Figure 2a shows the configuration of our refTOF-MS. The spectrometer consisted of a repeller electrode (4000 V), an extraction electrode (1500 V), three electrodes of an einzel lens (0, −2000, and 0 V), electrostatic deflectors (horizontal, vertical), a curved-field reflectron (offset 108 V; the voltage applied to the final electrode at the rear part was 3680 V), and the MCP. In refTOF-MS, primary ions formed by focusing femtosecond laser pulses are accelerated in the ion source, whose extraction field was 1389 V cm^{-1}. To reproduce the time-of-flight spectra of MMCs, we performed ion trajectory simulation using SIMION 3D™ version 8.0 (Scientific Instrument Services). The trajectory of DIA^{4+} is shown as a blue line in Figure 2a. Figure 2b shows the electrostatic potential felt by the primary ion, for example, DIA^{4+}, as a function of its flight time. If the primary ions are decomposed in the ion source, such as by an instantaneous Coulomb explosion,[2] their fragment ions are also accelerated as in the cases of primary ions. Thus, primary ions and their fragment ions formed in the ion source are spatially (temporally) separated by their mass-to-charge ratio in the first drift (electric field-free) region. For reference, the evolution of the velocity of DIA^{4+} is shown in Figure 2b. Supposing that ions are decomposed by metastable ion dissociation in the first drift region, the precursor ion and its product ions fly with the same velocity; for example, 87.2×10^3 m s^{-1} in the case

of DIA^{4+}. Once the precursor ion and its product ions are reflected in the curved-field reflectron, they are separated by their mass-to-charge ratio in the second drift region. Consequently, we can state that the primary ion is not fully decomposed in the first drift region if we detect it by ref-TOFMS. In other words, we can estimate the lower limit of the lifetime of a precursor ion that corresponds to the flight time between the ion source and the entrance of the reflectron in refTOF-MS. Based on the simulated results, DIA^{4+} is expected to spend 0.49, 11.90, 6.00, and 6.55 μs in the ion source, first drift region, curved-field reflectron, and second drift region, respectively. Since the experiments cannot measure each flight time, we compared the total flight time of DIA^{z+} (z = 1−4) obtained by experiments and simulations (Figure 2c). We also compared the flight times of fragment ions (C_2I^+, I^+, I^{2+}) formed in the ion source to further confirm the reproducibility of the simulation. We are confident that the ion trajectory simulations well reproduced the experiments because the coefficient of determination was unity (Figure 2c). We conclude that DIA^{4+} is intact for at least 12.4 μs since it was observed by refTOF-MS. Similarly, DIA^{z+} (z = 1−3) are intact for at least 24.8 (z =1), 17.5 (z =2), and 14.3 μs (z =3). It should be mentioned that we can increase or decrease the flight time by adjusting the acceleration and reflectron voltages without losing the focusing ability. We tried to make the flight time longer by decreasing the acceleration volage;

however, the decrease of the ion velocity resulted in the significant decrease of ion signal since the detection efficiency of a MCP is dependent of the impact speed of ions. We hope that we could try to use a mass spectrometer with a very long flight path such as a multi-turn time of flight mass spectrometer in future.

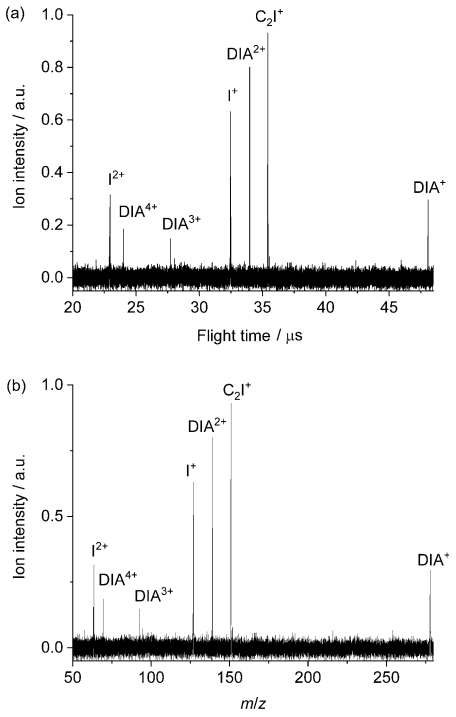

Figure 1. (a) Time-of-flight and (b) mass spectra of diiodoacetylene (5.0×10^{-4} Pa) ionized at 3.0×10^{14} W cm^{-2}. The spectrum was taken by a time-of-flight mass spectrometer equipped with a curved-field reflectron. DIA^{z+} denotes zth charged diiodoacetylene molecular cation.

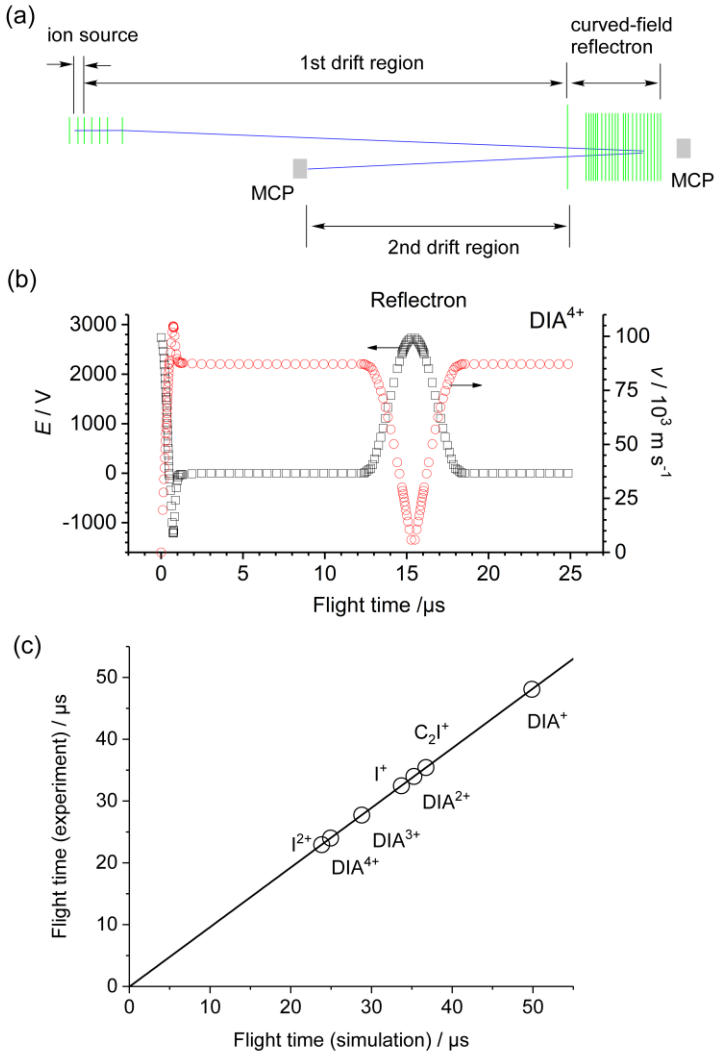

Figure 2. (a) Configuration of a time-of-flight mass spectrometer equipped with a curved-field reflectron. The trajectory of DIA^{4+} is shown as a blue line. MCP denotes a microchannel plane detector. (b) Electrostatic potential felt by DIA^{4+} (open squares) and velocity of DIA^{4+} (open circles) as a function of flight time. (c) Correlation between flight times obtained by experiments and simulations. A straight line was obtained by a least-squares method. The coefficient of determination was 1.0. DIA^{z+} denotes *z*th charged diiodoacetylene molecular cation.

3.2. Equilibrium Structure of the Electronic Ground State of MMCs. We previously reported the DFT calculations for the equilibrium structures of DIA^{z+} (z = 1−4).[29] It should be mentioned that DFT calculation was successful because the discrepancy in the $<S^2>$ between the calculated values using DFT and the theoretical values derived from S(S + 1) was small (<0.02) for the obtained equilibrium structures of the ground electronic state of DIA^{z+} (z =1−4). That for the triplet tetracation was relatively large (0.20) indicating the spin contamination effects due to mixing with some excited states of higher multiplicity. The molecular orbitals used as the active space and the energy levels of DIA and DIA^{4+} are shown in Figure 3. The energy gap between HOMO (5π, 6π) and LUMO (3σ) in neutral DIA was larger than those between occupied orbitals. In contrast, the energy gap between HOMO (3π, 4π) and LUMO (5π, 6π) in DIA^{4+} was comparable to those between occupied orbitals. These features strongly suggest that we should utilize the CASSCF method for MMCs to consider not only a single electron configuration but also electron configurations that include the excitations of electrons to energetically-close unoccupied orbitals. Molecular orbitals of DIA^{z+} (z = 0−4) at equilibrium structures calculated by CASSCF are compared in Figure S1. Although the equilibrium structure was not obtained for DIA^{5+} by the CASSCF method, the molecular orbitals of DIA^{5+}, which were calculated by the

CASSCF method for the fixed structure obtained by DFT theory as an optimized structure, are presented for reference in Figure S1. It should be mentioned that the energy of molecular orbitals is strongly dependent on whether MMCs are formed as odd-electron cation radicals or even-electron cations. The π-character orbitals (1π–6π) of neutral, dication, and tetracation were degenerated. In contrast, the energies of the π-character orbitals in cation radical, trication radical, and pentacation radical were well separated.

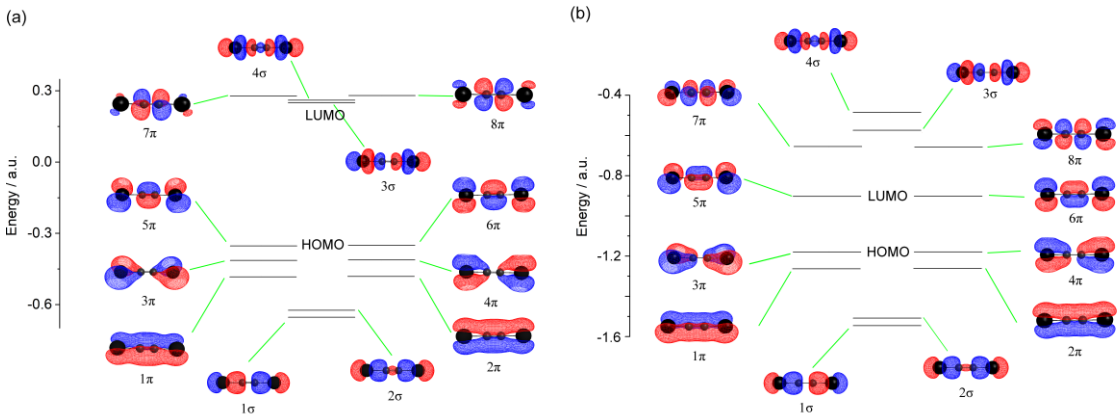

Figure 3. Molecular orbitals of (a) DIA and (b) DIA^{4+} at equilibrium configuration calculated by CASSCF.

Based on the energies of equilibrium structure calculated by the CASSCF method, the multiplicities of the electronic ground states were determined to be singlet (DIA, DIA^{4+}), doublet (DIA^{+}, DIA^{3+}), and triplet (DIA^{2+}) (Figure S2). The lowest energy level of DIA^{5+}, calculated by the CASSCF method without geometric optimization for

the structure obtained by DFT, was doublet, followed by quartet and sextet. Although several states are formed for each charge state, it might be expected that in this study there would be little likelihood of detecting the excited ions owing to their repulsive nature in the time scale of mass spectroscopic detection using a time-of-flight mass spectrometer. For example, the lifetime of the acetylene dication varied from pico- to microseconds.[39] Though the higher energy states of DIA are interesting, we consider the lowest energy state of MMCs in this study. The geometric parameters, Mulliken atomic charge, and relative energy of the electronic ground states of DIA are shown in Table 1. Table 2 shows four representative electron configurations of the equilibrium structure of the electronic ground states. In the cases of neutral and cation radicals, the coefficient of the most probable electron configuration was more than 0.9, whereas that of higher charge states became smaller as the charge number increased. Figure 4 shows the sum of the square of the coefficients of each charge state. It is evident that the electronic states of MMCs were not described by a single electron configuration as the charge number increased. However, the bond lengths calculated by CASSCF were not significantly different from those obtained by DFT (Table 1). The trend of bond length change was opposite between C-I and C-C bonds: as the charge number increased, the C-C bond lengthened whereas the C-I bond shortened. These changes indicate that as the charge number increases, the C-C

bond weakens but C-I bonds strengthen. Thus, we compared the vibrational frequencies of the equilibrium structures (Table 3). DIA, a four-atom molecule, has seven normal vibrations: ν_1 (C-C symmetric stretching), ν_2 (C-I symmetric stretching), ν_3 (C-I asymmetric stretching), ν_4 (doubly degenerated, C-C-H bending), ν_5 (doubly degenerated, I-C-C-I wagging). For the cases of a neutral molecule and cation radical, the calculated wavenumbers coincided well with those obtained by the experiments. As expected from the calculated bond lengths of the equilibrium structure, the wavenumbers of C-C stretching vibration (ν_1) decreased, whereas those of C-I stretching vibrations (ν_2 and ν_3) increased as an electron was removed from a neutral molecule. This trend is understood by the characteristics of molecular orbitals, from which electrons are removed. For the cases of cation radical, dication, trication radical, and tetracation, the removal of electrons from the 5π and 6π orbitals is an energetically favorable process. These orbitals are the superposition of bonding π orbitals in a C-C bond and lone-pair orbitals on I atoms. In other words, they are antibonding orbitals in a C-I bond, where nodes exist between carbon and iodine atoms. Therefore, removing electrons from the 5π and 6π orbitals strengthens C-I bonds but weakens a C-C bond. For the case of pentacation radical, the electron configuration with the largest coefficient (0.747) corresponded to the removal of four electrons from the 5π and 6π orbitals and one electron from the 4π orbital. This

electron configuration might contribute to the weakening of C-I bonds in pentacation radical. However, this electron configuration alone is presumably not enough to describe the instability of pentacation radical since DFT calculation predicted equilibrium structure. The electron configurations with the second (0.275) and third (0.184) largest coefficients obtained by CASSCF calculations corresponded to the excitation of electron(s) from the 3π (2π) orbital to the 5π (6π) orbital. Transfer of the electron(s) from the 3π (2π) orbital, where a node existed between carbon atoms (3π) or superimposed π orbitals in C-I and C-C bonds (2π), to the 5π (6π) orbital (the antibonding orbital in the C-I bond) is important in order to describe the weakness of C-I bonds of pentacation radical.

Table 1. Bond Length, Mulliken Atomic Charge, and Relative Energy of DIA^{z+} at Equilibrium Configuration Calculated by CASSCF and DFT[a]

	Bond length / Å				Mulliken atomic charge				Relative energy / eV	
	CASSCF		DFT		CASSCF		DFT		CASSCF	DFT
	C-I	C-C	C-I	C-C	C	I	C	I		
^{1}DIA	2.03	1.21	2.00	1.21	−0.154	0.154	−0.177	0.177	0	0
$^{2}DIA^{+}$	1.97	1.24	1.96	1.26	−0.074	0.574	−0.059	0.559	8.60	8.86
$^{3}DIA^{2+}$	1.94	1.26	1.92	1.26	−0.049	1.049	0.010	0.990	21.9	22.9
$^{2}DIA^{3+}$	1.92	1.30	1.90	1.30	0.022	1.478	0.086	1.414	40.8	43.2
$^{1}DIA^{4+}$	1.88	1.39	1.88	1.36	0.101	1.898	0.173	1.827	64.9	69.0
$^{2}DIA^{5+}$	b	b	2.02	1.36	b	b	0.229	2.271	97.0[c]	101

[a] 6-311G* basis set (CASSCF) and 6-31G basis set (DFT) were used.

[b] Not available

[c] Relative energy of DIA^{5+} was calculated by the CASSCF method without geometric optimization for the structure obtained by DFT calculations as an optimized structure.

Table 2. Four Largest Electron Configurations of the Electronic Ground States of DIA^{z+}

	Electron configuration[a]	Coefficient (C_f)	$\sum(C_f)^2$
^1DIA	222222220000	0.9470	0.9097
	222222200002	−0.0672	
	222222020020	−0.0672	
	220222220020	−0.0618	
$^2DIA^+$	2222222α0000	0.9385	0.8953
	2202222α2000	0.0766	
	2222220α2000	0.0659	
	22β222αα2000	−0.0654	
$^3DIA^{2+}$	222222αα0000	0.8938	0.8703
	2222αα220000	−0.2468	
	222022αα2000	−0.0725	
	220222αα0200	−0.0725	
$^2DIA^{3+}$	222222α00000	0.8601	0.8253
	222220α20000	0.2251	
	2222αβ2α0000	−0.1551	
	2222αα2β0000	−0.1040	
$^1DIA^{4+}$	222222000000	0.8330	0.7634
	222202200000	−0.1746	
	222220020000	−0.1746	
	2222αββα0000	0.0922	
$^2DIA^{5+}$	22222α000000	0.7477	0.6959
	22220α200000	0.2754	
	222α2β0α0000	0.1847	
	22202α020000	0.1635	

[a] The occupation of orbitals in the active space is shown. The orbitals, from left to right, correspond to 1σ, 2σ, 1π, 2π, 3π, 4π, 5π, 6π, 3σ, 4σ, 7π, and 8π shown in Figure 3. 0 and 2 imply unoccupied and doubly occupied orbitals, respectively, whereas α and β denote one electron with spin up or down, respectively.

Table 3. Vibrational Modes (in cm^{-1} unit) of DIA^{z+} at Equilibrium Configuration

		$\nu_1\ (\Sigma_g^+)$	$\nu_2\ (\Sigma_g^+)$	$\nu_3\ (\Sigma_u^+)$	$\nu_4\ (\Pi_g)$		$\nu_5\ (\Pi_u)$	
^1DIA	calcn.	2253	198.1	706.2	255.4	255.4	105.9	105.9
	exp.	2118[a]	190[a]	727[b]	296[a]		110[b]	
$^2DIA^+$	calcn.	2100	213.5	740.8	225.1	320.0	111.2	113.4
	exp.	1990[c]	234[c]/242[d]		214[c]/221[d]		94[c]/101[d]	
$^3DIA^{2+}$	calcn.	1887	218.3	808.4	303.3	303.3	126.6	126.6
$^2DIA^{3+}$	calcn.	1677	215.9	798.4	310.1	369.8	135.4	140.9
$^1DIA^{4+}$	calcn.	1217	220.9	850.4	384.8	384.8	154.7	154.7

[a] Data taken by Raman spectroscopy in benzene. Ref. 40-41

[b] Data taken by IR spectroscopy in gas phase. Ref. 42

[c] Data taken by emission spectroscopy ($A\ ^2\Pi_{g1/2} \rightarrow X\ ^2\Pi_{u1/2}$) in gas phase. Ref. 43

[d] Data taken by emission spectroscopy ($A\ ^2\Pi_{g3/2} \rightarrow X\ ^2\Pi_{u3/2}$) in gas phase. Ref. 43

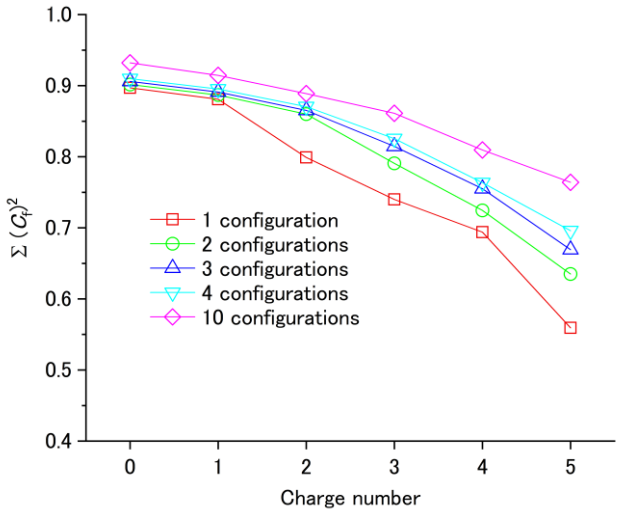

Figure 4. The sum of the square of the coefficients of electron configurations for the equilibrium configuration of DIA^{z+} (z = 0–4). The coefficients of DIA^{5+} were obtained for the fixed structure optimized by DFT calculation as an equilibrium structure.

The trends of Mulliken atomic charges calculated by the CASSCF method for the equilibrium structures of DIA and DIA^{z+} (z = 1−4) were similar to those obtained by DFT calculations (Table 1). In our previous study, we concluded that the tetracation remains metastable towards dissociation because of the localization of the positive charges (>90%) on the terminal iodine atoms, ensuring minimum Coulomb repulsion between adjacent atoms as well as maximum charge-induced attractive dipole interactions between iodine and carbon.[29] We can say that CASSCF calculations lead to the same conclusion about the the stability of MMCs at their equilibrium structures. In detail, the positive charges on carbon atoms calculated by CASSCF were smaller than those obtained by DFT, probably because multiple electron configurations are considered. For example, the electron configuration with the largest coefficient (0.83) for tetracation was the same as that of the single determinant used in the DFT calculation. The electron configurations with the second largest coefficient (−0.17) correspond to the excitation of an electron in the 3π (4π) orbital, which is a lone-pair orbital on I atoms, to the 5π (6π) orbital, which is the superposition of the bonding π orbital in the C-C bond and the lone-pair orbital on the I atom. The transfer of electrons from iodine atoms to carbon atoms neutralizes the positive charge on the latter. These contributions found by the CASSCF method would decrease the Coulomb repulsion between carbon atoms.

3.3. C-I Bond Elongation, Charge Redistribution, and Dissociation

DIA fragmentation is promoted by a C-I bond cleavage because the fragment ion distribution (C_2^+, C_2I^+, and C_2I^{2+}) indicates that the cleavage of the C-C bond is preceded by a C-I bond dissociation. Figure 5 shows the potential energy curves of DIA along the stretching coordinate of a C-I, where the remaining internuclear distances are kept fixed at their equilibrium distances. The potential minima corresponded to the equilibrium structure as listed in Table 1. In the cases of a neutral molecule and cation radical, the potential energy rises monotonically. For the cases of dication, trication radical, and tetracation, there are an energy barrier and a large activation energy for the reaction in both the expansion and contraction directions. The pentacation radical formed a repulsive potential curve along the C-I stretching coordinate. From the depth of the potential and zero-point energy (Table 4), the bond dissociation energies D_0s were estimated: 3.01 (^{1}DIA), 3.59 (^{2}DIA$^+$), 2.57 (^{3}DIA^{2+}), 1.82 (^{2}DIA^{3+}), and 1.61 eV (^{1}DIA^{4+}). The D_0 of ^{2}DIA$^+$ was larger than that of ^{1}DIA, which is consistent with the results of vibrational frequencies. We conclude that the bond dissociation energy is large enough to explain why DIA tetracation remains metastable towards dissociation.

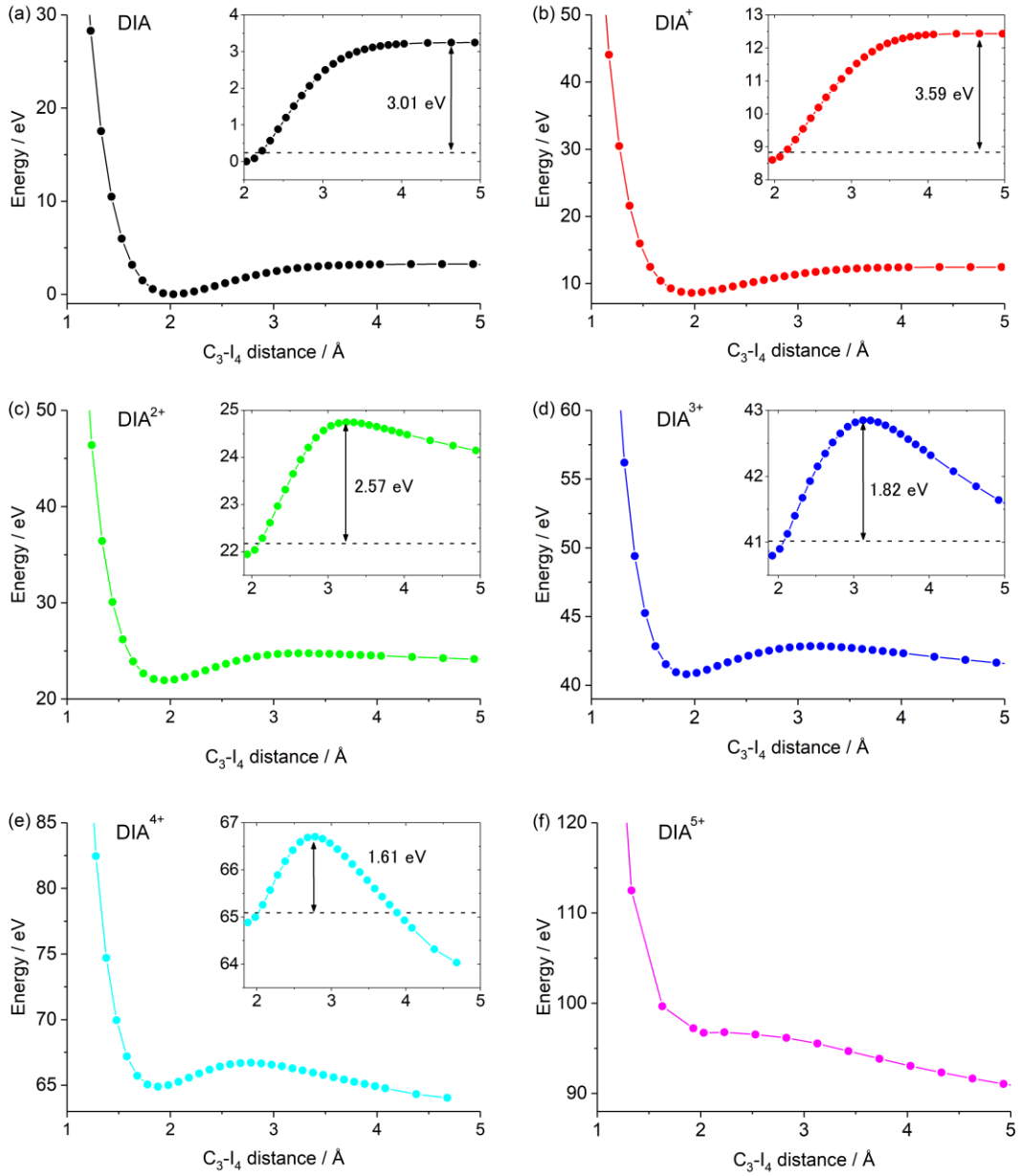

Figure 5. Potential energy curves of DIA (I_1-C_2-C_3-I_4) as a function of the C_3-I_4 distance: (a) ^{1}DIA, (b) ^{2}DIA$^+$, (c) ^{3}DIA^{2+}, (d) ^{2}DIA^{3+}, (e) ^{1}DIA^{4+}, (f) ^{2}DIA^{5+}. The remaining bond lengths are fixed at the equilibrium distances of DIA^{z+} ($z = 0–4$). In the case of ^{2}DIA^{5+}, the structure of I_1-C_2-C_3 was fixed at the structure optimized by DFT calculation as an equilibrium structure. Insets show the magnification of the peak of the potential barrier. Dashed horizontal line show the zero-point energy at equilibrium configuration.

Table 4. Zero-point Energy at Equilibrium Configuration, Dissociation Energy, and Kinetic Energy Release of DIA^{z+}

	Zero-point energy/ cm^{-1}	Dissociation energy / cm^{-1} (eV)	Kinetic energy release / eV
^{1}DIA	1940	2.424×10^{4} (3.01)	0.00 ($^{2}ICC + {}^{2}I$)
$^{2}DIA^{+}$	1912	2.896×10^{4} (3.59)	−0.65 ($^{1}ICC^{+} + {}^{2}I$)
			0.04 ($^{3}ICC^{+} + {}^{2}I$)
$^{3}DIA^{2+}$	1887	2.073×10^{4} (2.57)	0.65 ($^{1}ICC^{+} + {}^{1}I^{+}$)
			1.36 ($^{3}ICC^{+} + {}^{1}I^{+}$)
			2.01 ($^{1}ICC^{+} + {}^{3}I^{+}$)
			2.72 ($^{3}ICC^{+} + {}^{3}I^{+}$)
$^{2}DIA^{3+}$	1824	1.471×10^{4} (1.82)	3.16 ($^{2}ICC^{2+} + {}^{1}I^{+}$)
			4.13 ($^{4}ICC^{2+} + {}^{1}I^{+}$)
			4.52 ($^{2}ICC^{2+} + {}^{3}I^{+}$)
			5.49 ($^{4}ICC^{2+} + {}^{3}I^{+}$)
$^{1}DIA^{4+}$	1684	1.300×10^{4} (1.61)	11.2 ($^{2}ICC^{2+} + {}^{4}I^{2+}$)
			14.2 ($^{4}ICC^{2+} + {}^{4}I^{2+}$)
$^{2}DIA^{5+}$	a	a	17.3 ($^{3}ICC^{3+} + {}^{4}I^{2+}$)[b]
			17.7 ($^{1}ICC^{3+} + {}^{4}I^{2+}$)[b]

[a] Not available

[b] The relative energy (97.0 eV) shown in Table 1 was used for calculation.

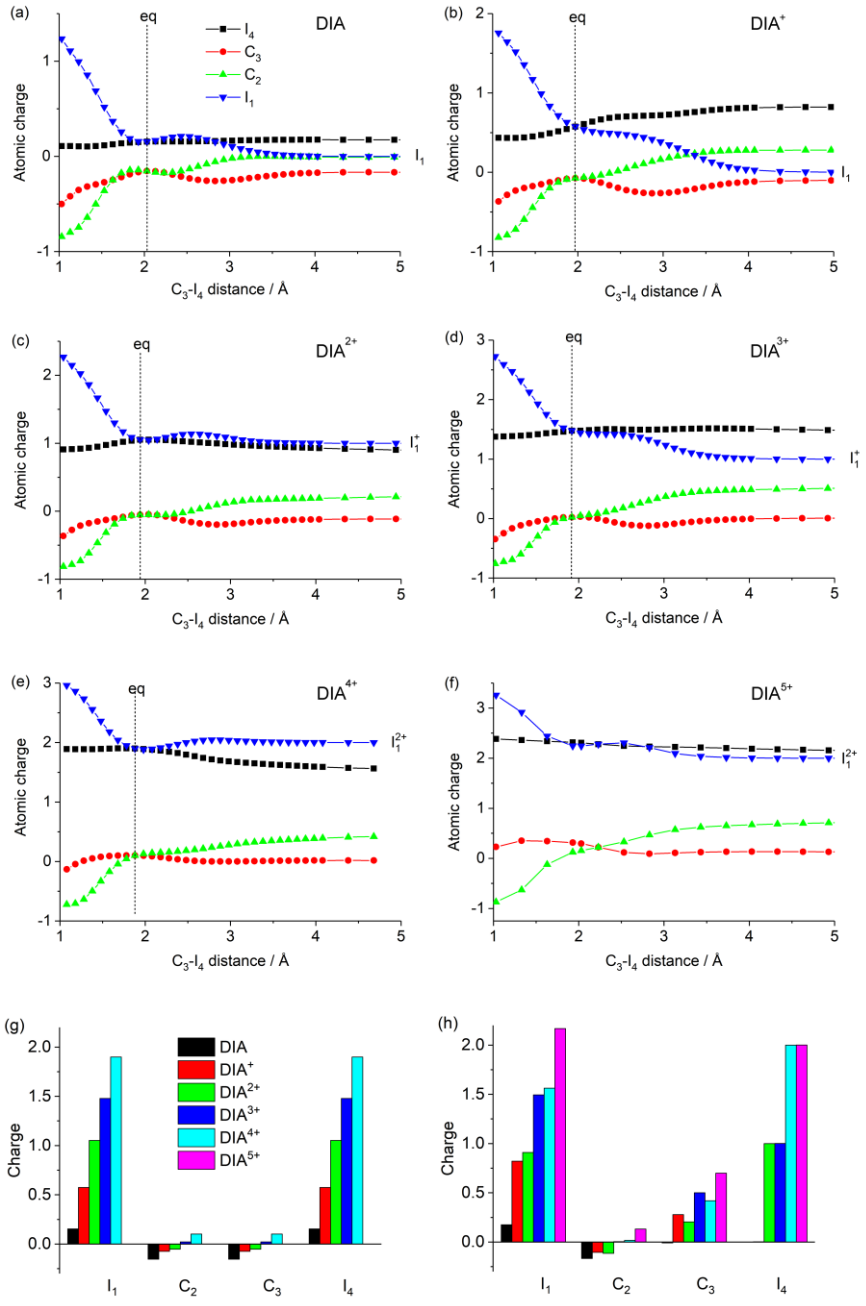

Figure 6. The evolution of the Mulliken atomic charge of DIA (I_1-C_2-C_3-I_4) along the C_3-I_4 stretching coordinate: I_1 (squares), C_2 (circles), C_3 (triangles), I_4 (inverted triangles). (a) ^{1}DIA, (b) ^{2}DIA$^+$, (c) ^{3}DIA^{2+}, (d) ^{2}DIA^{3+}, (e) ^{1}DIA^{4+}, (f) ^{2}DIA^{5+}. "eq" denotes the equilibrium C_3-I_4 distance for each charge state. Charge distributions at (g) the equilibrium C_3-I_4 distance and at (h) the C_3-I_4 distance elongated to 4.6 Å. The remaining bond lengths are fixed at their

equilibrium distances. In the case of $^{2}DIA^{5+}$, the structure of I_1-C_2-C_3 was fixed at the structure optimized by DFT calculation as an equilibrium structure.

Figure 6 shows the evolution of Mulliken atomic charges along the C-I stretching coordinate. Positive charges were dominantly localized on the iodine atoms at the equilibrium structure (Figure 6g). Based on the charge of the iodine atom when the length of the C-I bond became 4.6 Å, which is a fairly long distance compared with the equilibrium bond length, we can suggest the dissociation scheme forming ICC, ICC^{+}, ICC^{2+}, ICC^{3+}, I, I^{+}, or I^{2+} for each charge state (Scheme 1). These expected dissociation paths are reasonable because electrons stay in the fragment with higher ionization potential. As the C-I bond elongated, the positive charge was redistributed within the ICC fragment. We emphasize that the positive charge in the ICC fragment is again localized on the edge of the molecule as shown in Figure 6h.

$$^{1}ICCI \longrightarrow ICC + I$$
$$^{2}ICCI^{+} \longrightarrow ICC^{+} + I$$
$$^{3}ICCI^{2+} \longrightarrow ICC^{+} + I^{+}$$
$$^{2}ICCI^{3+} \longrightarrow ICC^{2+} + I^{+}$$
$$^{1}ICCI^{4+} \longrightarrow ICC^{2+} + I^{2+}$$
$$^{2}ICCI^{5+} \longrightarrow ICC^{3+} + I^{2+}$$

Scheme 1. Possible Charge Separation Reaction of DIA MMCs

To calculate the kinetic energy releases (KERs) in the possible dissociation paths, we performed CASSCF calculations for ICC and I separately, since the interaction between ICC and I at an infinite distance is considered negligible. We selected three π orbitals for the iodine atom and nine (six π and three σ) orbitals for ICC as the active space. KERs are defined as the difference between the energy of a saddle point and the total energy of the fragments. For the case of $^{2}DIA^{5+}$, the relative energy (97.0 eV) shown in Table 1 was used for the calculation. The KERs listed in Table 4 were dependent on the multiplicity of each fragment. The combinations that gave the lowest energy, i.e., the largest KER, were $^{3}ICC^{+}$ and ^{2}I ($^{2}DIA^{+}$), $^{3}ICC^{+}$ and $^{3}I^{+}$ ($^{3}DIA^{2+}$), $^{4}ICC^{2+}$ and $^{3}I^{+}$ ($^{2}DIA^{3+}$), $^{4}ICC^{2+}$ and $^{4}I^{2+}$ ($^{1}DIA^{4+}$), and $^{1}ICC^{3+}$ and $^{4}I^{2+}$ ($^{2}DIA^{5+}$). Since ICC^{3+} was not observed and ICC^{2+} was detected only as a minor product in the mass spectra, they should decompose by successive C-I bond dissociation.

Here we consider the molecular orbitals of $^{1}DIA^{4+}$ and $^{2}DIA^{3+}$ as representative examples to consider the dissociation paths of even-electron cations and odd-electron cation radicals, respectively. Their molecular orbitals at elongated geometries are shown in Figure 7. Table 5 shows three representative electron configurations of $^{1}DIA^{4+}$ and $^{2}DIA^{3+}$ at elongated geometries. Six orbitals were singly occupied in $^{1}DIA^{4+}$, whereas five orbitals were singly occupied in $^{2}DIA^{3+}$. We note that the π orbitals were degenerated in $^{1}DIA^{4+}$, while the energies

of some π orbitals (3π and 4π; 5π and 6π) were significantly separated in $^{2}DIA^{3+}$. Moreover, the energy of the 3σ orbital in $^{2}DIA^{3+}$ was shifted upward relative to those of the π orbitals.

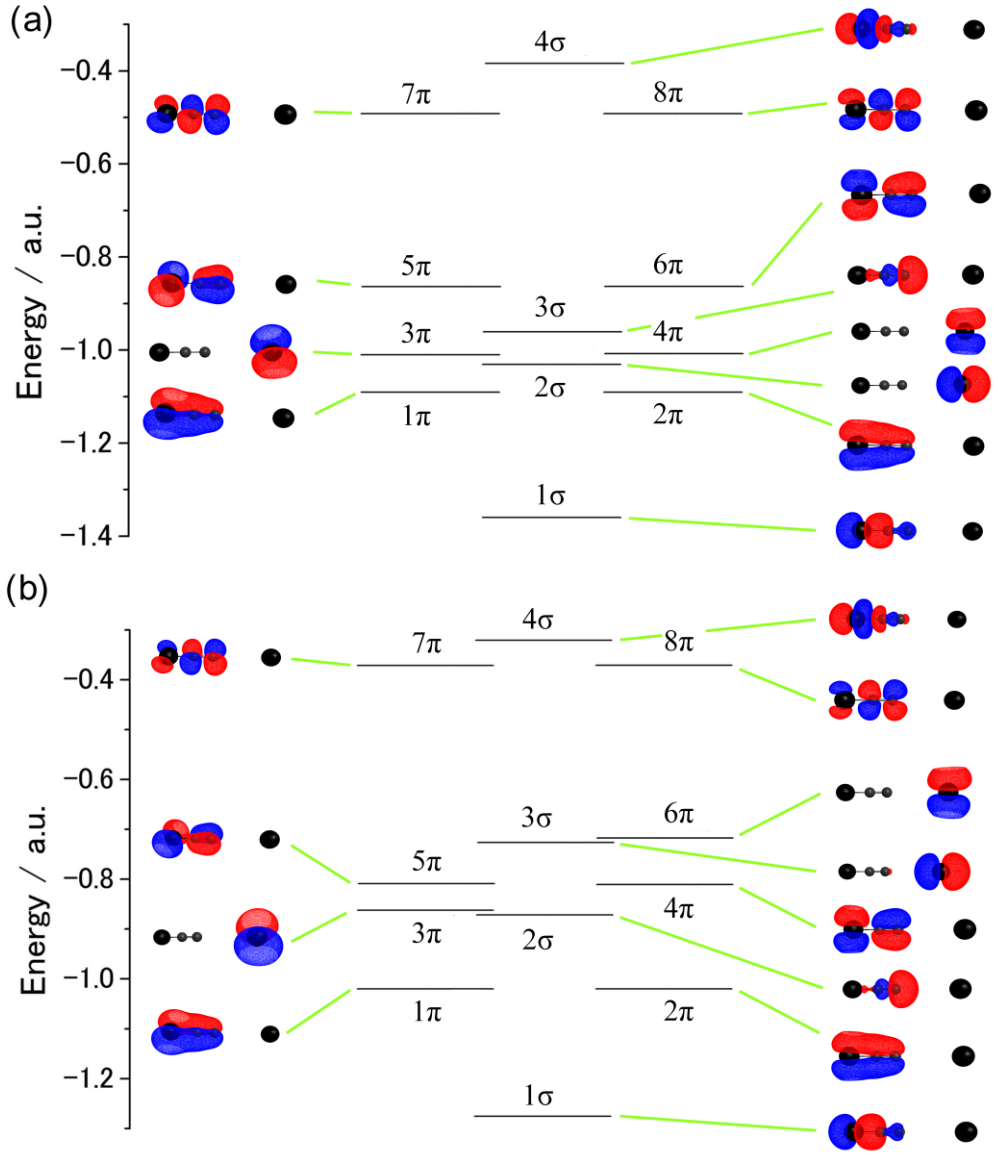

Figure 7. Molecular orbitals of (a) $^{1}DIA^{4+}$ (r (C_3-I_4) = 4.68 Å) and (b) $^{2}DIA^{3+}$ (r (C_3-I_4) = 4.92 Å) calculated by CASSCF.

Table 5. Three Largest Electron Configurations of the Electronic Ground States of $^{2}DIA^{3+}$ and $^{1}DIA^{4+}$ at Elongated C_3-I_4 Distance

DIA^{z+} (C_3-I_4 distance / Å)	Electron configuration[a]	Coefficient (C_f)	$\sum(C_f)^2$	Combination
$^{2}DIA^{3+}$	2α222ααββ000	0.6013	0.449	$^{4}ICC^{2+}+^{3}I^{+}$
(4.92)	2β222αααβ000	−0.2100		$^{2}ICC^{2+}+^{1}I^{+}$
	2α222βαβα000	−0.2088		$^{2}ICC^{2+}+^{1}I^{+}$
$^{1}DIA^{4+}$	2β22ββαααα000	0.4402	0.408	$^{4}ICC^{2+}+^{4}I^{2+}$
(4.68)	2α22ααβββ000	0.4402		$^{4}ICC^{2+}+^{4}I^{2+}$
	2α22βββαα000	−0.1441		$^{2}ICC^{2+}+^{2}I^{2+}$

[a] The occupation of orbitals in the active space is shown. From left to right, the orbitals correspond to 1σ, 2σ, 1π, 2π, 3π, 4π, 5π, 6π, 3σ, 4σ, 7π, and 8π shown in Figure 7. 0 and 2 imply unoccupied and doubly occupied orbitals, respectively, whereas α and β denote one electron with spin up or down, respectively.

In the case of $^{1}DIA^{4+}$, three molecular orbitals (2σ, 3π, 4π) originated from the 6p ($6p_x$, $6p_y$, $6p_x$) orbitals of the iodine atom (I_4). The remaining nine orbitals belonged to ICC: bonding σ orbitals in C-I bonds (1σ), superimposed π orbitals without a node in C-I and C-C bonds (1π, 2π), bonding σ orbitals in dissociated C-I bonds (3σ), the superposition of bonding π orbitals in a C-C bond and lone-pair orbitals on I atoms (5π, 6π), antibonding σ orbital in a C-I bond (4σ), antibonding π orbitals in a C-C bond (7π, 8π). The molecular orbitals were occupied by the same number of electrons but their spin directions were different in three representative electron configurations (Table 5). The degenerated electron configurations with the largest coefficient (0.44) were consisted of the molecular orbitals (2σ, 3π, 4π, localized on

iodine atom, I_4) occupied by the electrons with the same spin direction (β β β or α α α). In addition, they were consisted of the molecular orbitals (5π, 6π, 3σ, located on ICC) occupied by the electrons with the same spin direction (α α α or β β β). Obviously, the directions of spin in the 2σ, 3π, and 4π orbitals of I_4 were opposite to those in the 5π, 6π, and 3σ orbitals of ICC. Those electron configurations of $^1DIA^{4+}$ at elongated geometries are fairly described by the open-shell singlet corresponding to the combination of $^4ICC^{2+}$ and $^4I^{2+}$. This combination gave the largest KER (Table 4). Similarly, the electron configuration of $^1DIA^{4+}$ with the third largest coefficient (–0.14) is described by the combination of $^2ICC^{2+}$ and $^2I^{2+}$.

In the case of $^2DIA^{3+}$, three molecular orbitals (3π, 6π, 3σ) originated from 6p ($6p_x$, $6p_y$, $6p_x$) orbitals of the iodine atom (I_4), in which the 3π orbital was doubly occupied. The remaining nine orbitals belonged to ICC: bonding σ orbitals in C-I bonds (1σ), bonding σ orbitals in dissociated C-I bonds (2σ), superimposed π orbitals without a node in C-I and C-C bonds (1π, 2π), superposition of bonding π orbitals in a C-C bond and lone-pair orbitals on the I atoms (4π, 5π), antibonding σ orbital in a C-I bond (4σ), antibonding π orbitals in a C-C bond (7π, 8π). The electron configuration with the largest coefficient (0.60) consisted of the molecular orbitals (6π, 3σ, localized on iodine atom, I_4) occupied by the electrons with the same spin direction (β β). In addition, this electron configuration consisted of the molecular orbitals (2σ, 4π, 5π, located on ICC) occupied by the electrons with the same spin direction (α

α α). Obviously, the direction of spin in the 6π and 3σ orbitals of I_4 was opposite to that in the 2σ, 4π, and 5π orbitals of ICC. The electron configuration of $^2DIA^{3+}$ at elongated geometry corresponded to the combination of $^4ICC^{2+}$ and $^3I^+$. This combination gave the largest KER (Table 4). Similarly, the electron configurations of $^2DIA^{3+}$ with the second and third largest coefficients (–0.21) are described by the combination of $^2ICC^{2+}$ and $^1I^+$.

As mentioned above, two-body dissociation paths of DIA MMCs to C_2I^+ (C_2I^{2+}) and I^+ (I^{2+}) were well explained by CASSCF method whether MMCs are even-electron cations or odd-electron cation radicals. As for experiments, we reported the anisotropic emission of iodine ions from DIA, but the peak of iodine ions in mass spectra was too broad to resolve the dissociation channels.[28] Beside atomic ions, we detected C_2I^+ and C_2I^{2+} originated from two-body dissociation of DIA. C_2I^+ was observed as a single peak accompanying small side peaks. Double peaks of C_2I^{2+} were found as very minor products. Based on the kinetic energy of those fragment ions, we assumed the singly charged iodine as a counter ion, and thus the origins of those fragment ions were assigned to be DIA^{2+} and DIA^{3+}, respectively. Moreover, the presence of C_2^+ indicated the subsequent dissociation of C_2I^+ and/or C_2I^{2+}. Tracing the charge-state-dependent dissociation paths is very interesting, but the amount of those fragments was quite small. Further investigation about the origin of those fragment ions requires covariance mapping and/or coincidence spectroscopy.[2]

4. CONCLUSION

The present study shows the existence of a long-lived DIA tetracation that survives for at least 12 μs in the gas phase. Moreover, CASSCF calculations confirm the stability of multiply charged DIA by considering the near-degeneracy electron correlation. Since the removal of the electrons belonging to antibonding π orbitals in C-I bonds is an energetically favorable process, DIA shows a unique characteristic: C-I bonds become strong by stripping up to four electrons. In addition, the positive charges are localized on the terminal iodine atoms ensuring minimum Coulomb repulsions between atoms. Calculations of potential energy curves along the stretching coordinate of a C-I bond show that the dissociation energy (1.61 eV) is enough to explain the metastability of DIA tetracation. CASSCF calculations explain the absence of pentacation radical in a mass spectrum due to its repulsive nature. Sequential ionization of tetracation to pentacation radical would occur under intense femtosecond laser fields. However, the CASSCF method reveals that the large contributions of the electron configurations, in which electron excitations from bonding orbitals to antibonding orbitals of a C-I bond, lead to the instability of the DIA pentacation radical. DIA MMCs are interesting from many aspects; for example, a simple dissociation path of a linear molecule consists of only four atoms, and has long-lived states with different charges. These features motivate

further investigation into not only theoretical viewpoints of multiply charged ion chemistry but also experimental challenges such as spectroscopy, ionization-wavelength-dependent dissociations, and intermolecular reactions.

ASSOCIATED CONTENT

Supporting Information.

The Supporting Information is available free of charge via the Internet at http://pubs.acs.org/

Molecular orbitals of DIAs at equilibrium configuration. Energy level of DIAs at equilibrium configuration.

AUTHOR INFORMATION

Corresponding Authors

Kazuo Toyota

Department of Chemistry, Graduate School of Science, Osaka City University, 3-3-138 Sugimoto, Sumiyoshi-ku, Osaka 558-8585 Japan; orcid.org/0000-0003-4025-7217; Email: ktoyota@osaka-cu.ac.jp

Tomoyuki Yatsuhashi

Department of Chemistry, Graduate School of Science, Osaka City University, 3-3-138 Sugimoto, Sumiyoshi-ku, Osaka 558-8585 Japan; orcid.org/0000-0002-6810-7774; Email: tomo@osaka-cu.ac.jp

Authors

Takashi Kawaguchi

Department of Chemistry, Graduate School of Science, Osaka City University, 3-3-138 Sugimoto, Sumiyoshi-ku, Osaka 558-8585 Japan

Kosei Kitagawa

Department of Chemistry, Graduate School of Science, Osaka City University, 3-3-138 Sugimoto, Sumiyoshi-ku, Osaka 558-8585 Japan

Masatoshi Kozaki

Department of Chemistry, Graduate School of Science, Osaka City University, 3-3-138 Sugimoto, Sumiyoshi-ku, Osaka 558-8585 Japan

Keiji Okada

Department of Chemistry, Graduate School of Science, Osaka City University, 3-3-138 Sugimoto, Sumiyoshi-ku, Osaka 558-8585 Japan

Nobuaki Nakashima

Department of Chemistry, Graduate School of Science, Osaka City University, 3-3-138 Sugimoto, Sumiyoshi-ku, Osaka 558-8585 Japan

Notes

The authors declare no competing financial interest.

ACKNOWLEDGMENTS

The present research was supported by Grant for Basic Science Research Projects from The Sumitomo Foundation (200589) and by JST PRESTO program. We thank Mr. Kazuhiko Kondo of Thales Japan Inc. for his kind contribution to our laser system.

References

1. Nakashima, N.; Shimizu, S.; Yatsuhashi, T.; Sakabe, S.; Izawa, Y., Large molecules in high-intensity laser fields. *J. Photochem. Photobiol. C* **2000,** *1* (2), 131-143.

2. Yatsuhashi, T.; Nakashima, N., Multiple ionization and Coulomb explosion of molecules, molecular complexes, clusters and solid surfaces. *J. Photochem. Photobiol. C* **2018,** *34*, 52-84.

3. Pitzer, M.; Kastirke, G.; Kunitski, M.; Jahnke, T.; Bauer, T.; Goihl, C.; Trinter, F.; Schober, C.; Henrichs, K.; Becht, J. *et al.*, Absolute configuration from different multifragmentation pathways in light-induced Coulomb explosion imaging. *ChemPhysChem* **2016,** *17* (16), 2465-2472.

4. Burt, M.; Boll, R.; Lee, J. W. L.; Amini, K.; Kockert, H.; Vallance, C.; Gentleman, A. S.; Mackenzie, S. R.; Bari, S.; Bomme, C. *et al.*, Coulomb-explosion imaging of concurrent CH_2BrI photodissociation dynamics. *Phys. Rev. A* **2017,** *96* (4), 043415.

5. Hishikawa, A.; Matsuda, A.; Fushitani, M.; Takahashi, E. J., Visualizing recurrently migrating hydrogen in acetylene dication by intense ultrashort laser pulses. *Phys. Rev. Lett.* **2007,** *99* (25), 258302.

6. Endo, T.; Neville, S. P.; Wanie, V.; Beaulieu, S.; Qu, C.; Deschamps, J.; Lassonde, P.; Schmidt, B. E.; Fujise, H.; Fushitani *et al.*, Capturing roaming molecular fragments in real time. *Science* **2020,** *370*, 1072-1077.

7. Lee, J. W. L.; Kockert, H.; Heathcote, D.; Popat, D.; Chapman, R. T.; Karras, G.; Majchrzak, P.; Springate, E.; Vallance, C., Three-dimensional covariance-map imaging of molecular structure and dynamics on the ultrafast timescale. *Commun Chem* **2020,** *3*, 72.

8. Ledingham, K. W. D.; Singhal, R. P.; Smith, D. J.; McCanny, T.; Graham, P.; Kilic, H. S.; Peng, W. X.; Wang, S. L.; Langley, A. J.; Taday, P. F. *et al.*, Behavior of polyatomic molecules in intense infrared laser beams. *J. Phys. Chem. A* **1998,** *102* (18), 3002-3005.

9. Vekey, K., Multiply charged ions. *Mass Spectrom. Rev.* **1995,** *14* (3), 195-225.

10. Schroder, D.; Schwarz, H., Generation, stability, and reactivity of small, multiply charged ions in the gas phase. *J. Phys. Chem. A* **1999,** *103* (37), 7385-7394.

11. Schröder, D., Coulomb explosions and stability of multiply charged ions in the gas phase. *Angew. Chem. Int. Ed.* **2004,** *43* (11), 1329-1331.

12. Böhme, D. K., Multiply-charged ions and interstellar chemistry. *Phys. Chem. Chem. Phys.* **2011,** *13* (41), 18253-18263.

13. Lammertsma, K.; Schleyer, P. V.; Schwarz, H., Organic dications: gas phase experiments and theory in concert. *Angew. Chem. Int. Ed.* **1989,** *28* (10), 1321-1341.

14. Hammami, H.; Yazidi, O.; Rhouma, M. B.; Al Mogren, M. M.; Hochlaf, M., Theoretical investigations of the IO,$^{q+}$ (q=2, 3, 4) multi-charged ions: Metastability, characterization and spectroscopy. *J. Chem. Phys.* **2014,** *141* (1), 014302.

15. Wong, M. W.; Nobes, R. H.; Radom, L., Remarkably stable trications and tetracations - the triheliomethyl trication ($CHe_3\bullet^{3+}$) and tetraheliomethane tetracation (CHe_4^{4+}). *J. Chem. Soc. Chem. Comm.* **1987**, 233-234.

16. Ito, A.; Taniguchi, A.; Yoshizawa, K.; Tanaka, K.; Yamabe, T., Ab initio CASSCF study on doublet and quartet states of 1,3,5-tris(methylene)benzene and 1,3,5-benzenetriamine trication. *Bull. Chem. Soc. Jpn.* **1998,** *71* (2), 337-343.

17. Brites, V.; Franzreb, K.; Harvey, J. N.; Sayres, S. G.; Ross, M. W.; Blumling, D. E.; Castleman, A. W.; Hochlaf, M., Oxygen-containing gas-phase diatomic trications and tetracations: ReO^{z+}, NbO^{z+} and HfO^{z+} (z = 3, 4). *Phys. Chem. Chem. Phys.* **2011,** *13* (33), 15233-15243.

18. Gutsev, G. L.; Pena, H. A. L.; McPherson, S. L.; Boateng, D. A.; Ramachandran, B. R.; Gutsev, L. G.; Tibbetts, K. M., From Neutral Aniline to Aniline Trication: A Computational and Experimental Study. *J. Phys. Chem. A* **2020,** *124* (16), 3120-3134.

19. Radom, L.; Gill, P. M. W.; Wong, M. W.; Nobes, R. H., Multiply-charged cations: remarkable structures and stabilities. *Pure Appl. Chem.* **1988,** *60* (2), 183-188.

20. Gutsev, G. L.; McPherson, S. L.; Pena, H. A. L.; Boateng, D. A.; Gutsev, L. G.; Ramachandran, B. R.; Tibbetts, K. M., Dissociation of Singly and Multiply Charged Nitromethane Cations: Femtosecond Laser Mass Spectrometry and Theoretical Modeling. *J. Phys. Chem. A* **2020,** *124* (37), 7427-7438.

21. Sairam, T.; Kumar, A.; Safvan, C. P., Can substitution accomplish intact polycationic stability in polyatomic molecules? Illustration with acetylene molecule. *J. Mol. Struct.* **2015,** *1099*, 348-350.

22. Mathur, D., Multiply charged molecules. *Phys. Rep.* **1993,** *225* (4), 193-272.

23. Mathur, D., Structure and dynamics of molecules in high charge states. *Phys. Rep.* **2004,** *391* (1-2), 1-118.

24. Bursey, M. M.; Rogerson, P. F.; Bursey, J. M., Quadruply charged ions in mass spectrum of ovalene. *Org. Mass Spectrom.* **1970,** *4*, 615-617.

25. Kingston, R. G.; Guilhaus, M.; Brenton, A. G.; Beynon, J. H., Multiple ionization, charge separation and charge stripping reactions involving polycyclic aromatic compounds. *Org. Mass Spectrom.* **1985,** *20* (6), 406-412.

26. Bhardwaj, V. R.; Corkum, P. B.; Rayner, D. M., Internal laser-induced dipole force at work in C_{60} molecule. *Phys. Rev. Lett.* **2003,** *91* (20), 203004.

27. Yatsuhashi, T.; Nakashima, N., Formation and fragmentation of quadruply charged molecular ions by intense femtosecond laser pulses. *J. Phys. Chem. A* **2010,** *114* (28), 7445-7452.

28. Yatsuhashi, T.; Mitsubayashi, N.; Itsukashi, M.; Kozaki, M.; Okada, K.; Nakashima, N., Persistence of iodines and deformation of molecular structure in highly charged diiodoacetylene: anisotropic carbon ion emission. *ChemPhysChem* **2011,** *12* (1), 122-126.

29. Yatsuhashi, T.; Toyota, K.; Mitsubayashi, N.; Kozaki, M.; Okada, K.; Nakashima, N., Intact four-atom organic tetracation stabilized by charge localization in the gas phase. *ChemPhysChem* **2016,** *17* (19), 2977-2981.

30. Kitashoji, A.; Fujihara, A.; Yoshikawa, T.; Yatsuhashi, T., The Smallest Aromatic Tetracation Produced in Gas Phase by Intense Femtosecond Laser Pulses. *Chem. Lett.* **2019,** *48* (12), 1472-1475.

31. Mitsubayashi, N.; Yatsuhashi, T.; Tanaka, H.; Furukawa, S.; Kozaki, M.; Okada, K.; Nakashima, N., Anisotropic Coulomb explosion of acetylene and diacetylene derivatives. *Int. J. Mass Spectrom.* **2016,** *403*, 43-52.

32. Kitashoji, A.; Yatsuhashi, T., Definitive production of intact organic pentacation radical: Octafluoronaphthalene ionized in intense femtosecond laser fields. *Chem. Phys.* **2019,** *526*, 110465.

33. Roos, B. O.; Taylor, P. R.; Siegbahn, P. E. M., A Complete Active Space SCF Method (CASSCF) Using a Density-Matrix Formulated Super-CI Approach. *Chem. Phys.* **1980,** *48* (2), 157-173.

34. Nelson, D. J.; Blue, C. D.; Brown, H. C., Hydroboration Kinetics .5. Kinetics of the Reaction of 9-Borabicyclo[3.3.1]Nonane with Representative Haloalkynes in Carbon-Tetrachloride - the Effect of Halogen Substitution Upon the Stoichiometry and Rate of Hydroboration. *J. Am. Chem. Soc.* **1982,** *104* (18), 4913-4917.

35. Kitashoji, A.; Yoshikawa, T.; Fujihara, A.; Kamamori, T.; Nashima, S.; Yatsuhashi, T., Selection of a Single Isotope of Multiply Charged Xenon ($^{A}Xe^{z+}$, A = 128-136, z = 1-6) by Using a Bradbury-Nielsen Ion Gate. *ChemPhysChem* **2017,** *18* (15), 2007-2011.

36. Kitashoji, A.; Kitagawa, K.; Fujihara, A.; Yatsuhashi, T., Charge Transfer and Metastable Ion Dissociation of Multiply Charged Molecular Cations Observed by Using Reflectron Time-of-Flight Mass Spectrometry. *ChemPhysChem* **2020,** *21* (9), 847-852.

37. Hankin, S. M.; Villeneuve, D. M.; Corkum, P. B.; Rayner, D. M., Nonlinear ionization of organic molecules in high intensity laser fields. *Phys. Rev. Lett.* **2000,** *84* (22), 5082-5085.

38. Barca, G. M. J.; Bertoni, C.; Carrington, L.; Datta, D.; De Silva, N.; Deustua, J. E.; Fedorov, D. G.; Gour, J. R.; Gunina, A. O.; Guidez, E. *et al.*, Recent developments in the general atomic and molecular electronic structure system. *J. Chem. Phys.* **2020,** *152* (15), 154102.

39. Alagia, M.; Callegari, C.; Candori, P.; Falcinelli, S.; Pirani, F.; Richter, R.; Stranges, S.; Vecchiocattivi, F., Angular and energy distribution of fragment ions in dissociative double photoionization of acetylene molecules at 39 eV. *J. Chem. Phys.* **2012,** *136* (20), 204302.

40. Klaboe, P.; Kloster-Jensen, E.; Christensen, D. H.; Johnsen, I., The vibrational spectra of dichloro-, dibromo-, diiodo-, bromochloro- and chloroiodoacetylene. *Spectrochim. Acta A* **1970,** *26* (7), 1567-1580.

41. Klosterj.E, Preparation and Spectra of Pure Hetero and Homo Dihaloacetylenes. *J. Am. Chem. Soc.* **1969,** *91* (20), 5673-5674.

42. Christensen, D. H.; Stroyer-Hansen, T.; Klaboe, P.; Kloster-Jensen, E.; Tucker, E. E., The vibrational spectra of bromoiodoacetylene force constants of six dihaloacetylenes. *Spectrochim. Acta A* **1972,** *28* (5), 939-951.

43. Klapstein, D.; Maier, J. P.; Zambach, W., Emission-Spectra of Rotationally Cooled Dihaloacetylene Cations in the Gas Phase: $\tilde{A}\ ^2\Pi_{\Omega,g} \rightarrow X\ ^2\Pi_{\Omega,u}$ Band Systems. *Chem. Phys.* **1983,** *77* (3), 463-475.

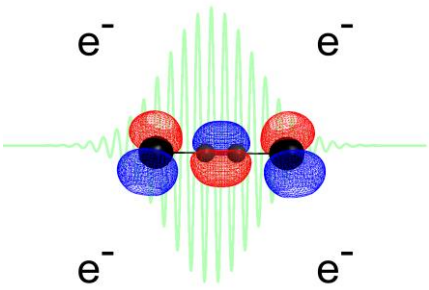

TOC Graphic